

Research Article

Enhanced Stem Cell Osteogenic Differentiation by Bioactive Glass Functionalized Graphene Oxide Substrates

Xiaoju Mo,^{1,2} Yan Wei,¹ Xuehui Zhang,³ Qing Cai,⁴ Yang Shen,⁵ Xiaohan Dai,⁶ Song Meng,¹ Xing Liu,¹ Yun Liu,¹ Zhewen Hu,¹ and Xuliang Deng^{1,7,8}

¹Department of Geriatric Dentistry, Peking University School and Hospital of Stomatology, Beijing 100081, China

²Department of Prosthodontics, Peking University School and Hospital of Stomatology, Beijing 100081, China

³Department of Dental Materials, Peking University School and Hospital of Stomatology, Beijing 100081, China

⁴State Key Laboratory of Organic-Inorganic Composites, Key Laboratory of Carbon Fiber and Functional Polymers, Ministry of Education, Beijing University of Chemical Technology, Beijing 100029, China

⁵State Key Laboratory of New Ceramics and Fine Processing and Department of Materials Science and Engineering, Tsinghua University, Beijing 100084, China

⁶Key Laboratory of Zoonosis, Ministry of Education, Institute of Zoonosis, College of Veterinary Medicine, Jilin University, Changchun 130062, China

⁷National Engineering Laboratory for Digital and Material Technology of Stomatology, Beijing 100081, China

⁸Beijing Laboratory of Biomedical Materials, Peking University School and Hospital of Stomatology, Beijing 100081, China

Correspondence should be addressed to Xuliang Deng; kqdengxuliang@bjmu.edu.cn

Received 30 March 2016; Accepted 19 May 2016

Academic Editor: Shuai Zhang

Copyright © 2016 Xiaoju Mo et al. This is an open access article distributed under the Creative Commons Attribution License, which permits unrestricted use, distribution, and reproduction in any medium, provided the original work is properly cited.

An unmet need in engineered bone regeneration is to develop scaffolds capable of manipulating stem cells osteogenesis. Graphene oxide (GO) has been widely used as a biomaterial for various biomedical applications. However, it remains challenging to functionalize GO as ideal platform for specifically directing stem cell osteogenesis. Herein, we report facile functionalization of GO with dopamine and subsequent bioactive glass (BG) to enhance stem cell adhesion, spreading, and osteogenic differentiation. On the basis of graphene, we obtained dopamine functionalized graphene oxide/bioactive glass (DGO/BG) hybrid scaffolds containing different content of DGO by loading BG nanoparticles on graphene oxide surface using sol-gel method. To enhance the dispersion stability and facilitate subsequent nucleation of BG in GO, firstly, dopamine (DA) was used to modify GO. Then, the modified GO was functionalized with bioactive glass (BG) using sol-gel method. The adhesion, spreading, and osteoinductive effects of DGO/BG scaffold on rat bone marrow mesenchymal stem cells (rBMSCs) were evaluated. DGO/BG hybrid scaffolds with different content of DGO could influence rBMSCs' behavior. The highest expression level of osteogenic markers suggests that the DGO/BG hybrid scaffolds have great potential or elicit desired bone reparative outcome.

1. Introduction

Graphene oxide (GO), a two-dimensional monolayer of carbon atoms intimately packed into a honeycomb lattice, has shown great promise for biomedical applications [1, 2], such as cell imaging [3], drug delivery [4, 5], and biomedical device [5, 6]. Furthermore, due to its unique nanostructures, remarkable mechanical properties, and large surface area [7–9], GO has gained tremendous attentions as a new nanoplatform for stem cell culture. Lee et al. indicated that

GO substrates could promote adipogenic differentiation of MSCs because of their high affinity to insulin [10]. Kim et al. demonstrated that GO substrates provide a suitable environment for ASCs adhesion, proliferation, and differentiation with presence of osteogenic chemical inducers [11, 12]. Recent work also demonstrated that GO can act as both an effective reinforcement and a bioactivator of biopolymers such as gelatin [13] and chitosan [14], offering the biopolymer-GO composites the possibility to manipulate bone cells behavior. However, in terms of stem cells osteogenesis, it remains

a great challenge to functionalize GO as ideal substrate for the effective specification of stem cell fate to enhance bone repair.

Bioactive glasses (BG), with biomimetic composition and significant degradation [15], have been contemporarily confirmed to possess high efficiency in bonding with bone. *In vivo* experiments results showed that implanted BG produced no systemic or local toxicity [16, 17], no inflammatory affection, and no repulsive response. Some *in vitro* studies suggested that the bioactivity of BG was associated with the formation of a crystalline hydroxyapatite surface layer and controlled release of ionic dissolution products [18, 19]. Furthermore, these ion dissolution and release of BG could exert a genetic control over the osteoblast cell cycle and the rapid expression of osteogenic genes [20, 21]. These discoveries have stimulated more extensive investigations of BG utilization for bone defect repair. BG decoration on carbon fibers has been demonstrated to promote hydroxyapatite nucleation, biomineralization, and cellular ALP activity [22]. BG incorporation in PLGA was also reported to induce BG-dose-dependent cell proliferation and ALP expression [23]. As such, we hypothesized that the BG might present as a prospective candidate to functionalize GO so as to provide effective environments to modulate structure and function of GO and facilitate stem cells' osteogenic differentiation.

In this study, we designed and fabricated DGO/BG hybrid scaffold using sol-gel method as osteoinductive substrates to manipulate stem cell fate. SEM, Raman, and EDS characterization confirmed the incorporation of BG on GO without compromising their characteristic bands. The cellular activities analysis demonstrated that DGO/BG hybrid scaffolds could significantly promote the adhesion, spreading, and osteogenic differentiation of mesenchymal stem cells, due to their unique nanoscale topography, biomimetic composition, and mechanical cues.

2. Materials and Methods

2.1. Preparation and Characterization of Graphene. Graphene oxide (GO) and its reduzate have been successfully prepared using an improved Hummers' method [24] and a reduction process using hydrazine hydrate and a chemical method for the simultaneous reduction and surface functionalization of GO using dopamine hydrochloride. TEM (HRTEM, H-7650B, Hitachi, Japan) was chosen to observe the structure and morphology of the samples. The composition and phase purity of the products were examined by X-ray diffraction spectroscopy (XRD, Rigaku D/max 2500 VB2+/PC, Japan), Raman spectra (LabRAM HR Evolution, HORIBA Jobin Yvon, France), and Fourier transform infrared spectroscopy (FTIR, Avatar 360, Nicolet Co., USA).

2.2. Synthesis and Characterization of Dopamine Functionalized Graphene Oxide/Bioactive Glass (DGO/BG). DGO/BG composite with 1 wt.% and 5 wt.% GO was synthesized by sol-gel-melting method through the following steps just as Figure 1. Tetraethoxysilane (TEOS, Aldrich, USA), calcium

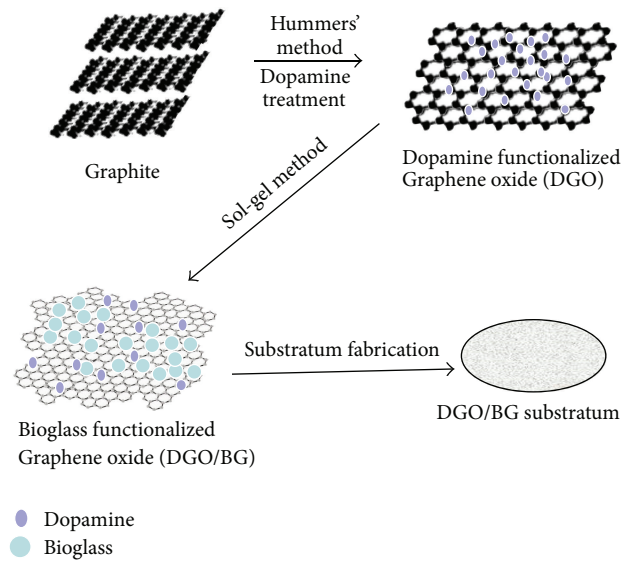


FIGURE 1: Schematic of process to synthesis DGO/BG by sol-gel-melting method in this study.

nitrate tetrahydrate (CN, Aldrich, USA), and triethyl phosphate (TEP, Aldrich, USA) were used to prepare 58S type BG by sol-gel solution. Briefly, TEP was added into a mixed solvent of distilled water, absolute ethyl alcohol, and ammonia water and stirred at 80°C for 24 h to obtain a hydrolyzed TEP solution. CN and TEOS were then dissolved into the hydrolyzed TEP solution and stirred continuously at room temperature for 120 h to generate a sol-gel solution. The DGO was dissolved in dimethylformamide (DMF, analytic pure, 99.5 wt.%, Tianjin Fine Chemical Co., China), followed by ultrasonication for 2 h. The prepared sol-gel solution was added into the solution of DGO to a total concentration of 1 wt.% and 5 wt.% DGO with different ratios. After 2 h of magnetic stirring, suspensions were dried on a hotplate at 80°C for 12 h. The composite was carbonized at 300°C for 1 h, 750°C for 2 h, and then at 1000°C for 3 h in N₂ atmosphere. Surface topography and elementary composition were observed by SEM and EMAX EX-300 system (Horiba, Japan) to confirm the successful reduction of resulting material as well as its immobilization with dopamine.

2.3. Preparation of DGO/BG-Based Substrates. Coating of glass coverslips with DGO/BG was performed as described below. In order to clean substrate, the glass coverslip with 14 mm diameter was first immersed into the piranha solution (hydrogen peroxide/sulfuric acid with the volumetric ratio of 1:3) for 10 minutes at 120°C, rinsed with ethanol and water for 5 minutes, and then blown dried by nitrogen gas at room temperature. Then the coverslip was immersed in 3% toluene solution of 3-aminopropyltriethoxysilane (3-APTES) for 30 min for functionalization. At last, it was baked with nitrogen at 125°C after being rinsed with toluene, ethanol, and water for 5 minutes again. 30 μL DGO/BG was uniformly coated on a coverslip surface by Spin Processor (Smart Coater 100, Analysis China Co., LTD) and then dried with

TABLE 1: Primers sequences utilized for real time RT-PCR.

| Target gene | Forward primer sequence (5'-3') | Reverse primer sequence (5'-3') |
|-------------|---------------------------------|---------------------------------|
| BMP2 | TGCTCAGCTTCCATCACGAAG | TCTGGAGCTCTGCAGATGTGA |
| BSP | GAGAACGCCACACTCTCAGG | GAGCCTTGCCCTCTGCATCT |
| OPN | TTTGCTTTTGCCGTGTTCCGGC | AGTCATCCGTTTCTTCAGAGGAC |
| RUNX2 | AATGCCTCCGCTGTTATG | TTCTGTCTGTGCCTTCTTG |

high temperature. The other samples were handled with the same way. Finally, substrates coated with these composite nanomaterial come into being four different samples: (i) functionalized graphene oxide with dopamine (DGO), (ii) 1 wt.% DGO/BG, (iii) 5 wt.% DGO/BG, and (iv) BG.

2.4. Cell Cultures and Conditions. Rat bone marrow mesenchymal stem cells (rBMSCs, Cyagen Biosciences, Inc., China) were routinely maintained in mesenchymal stem cell basal medium supplemented with 10% fetal bovine serum (FBS), 100 IU/mL penicillin-streptomycin, and 2 mM glutamine (Cyagen Biosciences, Inc., China) at 37°C in a humidified atmosphere of 5 wt.% CO₂ in air. Cells were seeded at 2.5×10^4 cells per cm² after two passages.

2.5. Immunofluorescence Staining for Cell Adhesion, Spreading, and Osteogenic Differentiation. Initial adhesion can be measured in early time ranging from 2 h to 1 d and the osteogenic differentiation usually in 7 d [25–27]. To assess the initial adhesion and osteogenic differentiation of rBMSCs, the cells were incubated with DGO/BG disks for 3 h, 1 d, and 7 d. Immunocytochemistry samples were harvested at each time point and then cells were fixed with 4.0% (w/v) paraformaldehyde for 30 min, permeabilized with 0.1 wt.% (w/v) TritonX-100 for 10 min, and blocked with 3 wt.% bovine serum albumin (BSA) for 1 h at room temperature. Samples were incubated with primary antibodies in 1 wt.% BSA for 2 h against BMP2 (abcam, ab14933), OPN (abcam, ab8448), RUNX2 (abcam, ab76956), and/or vinculin (abcam, ab18058). After removing the primary antibody, samples were incubated with secondary antibodies for 1 h at room temperature: goat anti-rabbit IgG H&L (TRITC) preadsorbed (abcam, ab50598) and goat anti-mouse IgG H&L (FITC) (abcam, ab6785). Then cells were treated with Phalloidin-Atto 565 (Sigma) for 1 h at room temperature and then stained with DAPI (Roche) for 10 min. The figures were captured by laser scanning confocal microscopy (Zeiss, LSM 780, Germany). DAPI was used to quantify cell number. The initial adhesion was evaluated by counting the number of live cells per unit area on each substrate and each group was repeated for three times.

2.6. Quantitative Real-Time PCR Analysis. rBMSCs were harvested after 7 days by TRIzol (Invitrogen) cultured on different samples. Then the isolated RNA was reverse-transcribed into cDNA utilizing the Reverse Transcription System (Promega, Madison, WI) with the manufacturer's instructions (Toyobo). Bone morphogenetic protein 2 (BMP2), bone sialoprotein (BSP), runt-related transcription

factor 2 (RUNX2), and osteopontin (OPN) were performed on the Applied ABI PRISM 7500 Real Time PCR System (Applied Biosystems, Foster City, CA) utilizing the QuantiTect SYBR Green Kit (Qiagen). The primer sequences of osteogenic genes are listed in Table 1.

2.7. Statistical Analysis. Fluorescence microscopy images were analyzed utilizing Matlab (MathWorks, Inc., R2011b) software. All quantitative data were expressed as mean \pm standard deviation (SD). The one-way ANOVA was performed for statistical analysis. Differences between groups of $*p < 0.05$ were considered statistically significant and $**p < 0.01$ was considered highly significant.

3. Results

3.1. Characteristics of Graphene. TEM images and digital photographs of graphene before and after the modification are shown in Figure 2(a). The GO sheets and DGO were smooth with folded shapes at the edges and aqueous dispersions of DGO showed a homodisperse state (Figure 2(a)(A), (B)). While following the chemical reduction, G sheets displayed a crumpled and wrinkled structure and the aqueous dispersions appeared to precipitate (Figure 2(a)(C)).

The composition and phase purity of the products were examined by XRD (Figure 2(b)). After reduction and modification, the typical GO peak at 11.28° disappears, and a new broad diffraction peak appears at 25°, corresponding to a decrease of interlayer spacing from 0.78 nm to 0.39 nm. Further characterization of the products was carried out by Raman. GO showed a D band at 1336 cm⁻¹ and G band at 1586 cm⁻¹, respectively. After modification and reduction of GO, the intensity ratio of the D band and G band (ID/IG) increased significantly (Figure 2(c) and Supplementary Figure S1 in Supplementary Material available online at <http://dx.doi.org/10.1155/2016/5613980>). FTIR was also used to characterize the products in Figure 2(d). The FTIR spectra of GO and DGO showed broad bands ranging from 3400 to 3500 cm⁻¹. The oxygen-containing functional groups of GO were revealed by the bands at 1054, 1226, 1617, and 1719 cm⁻¹.

3.2. Characterization of DGO/BG. SEM images showed topography and distribution of pure BG and BG in DGO/BG composites with different loading ratio and reaction temperature (Figures 3 and 4(a), Supplementary Figure S2). In all cases the BG particles showed a round shape. As indicated, BG particles only emerged above reaction temperature of 600°C with sol-gel method (Figure 3(a)(A)). At 1000°C, even distribution of BG particles with diameter ranging from 50 to

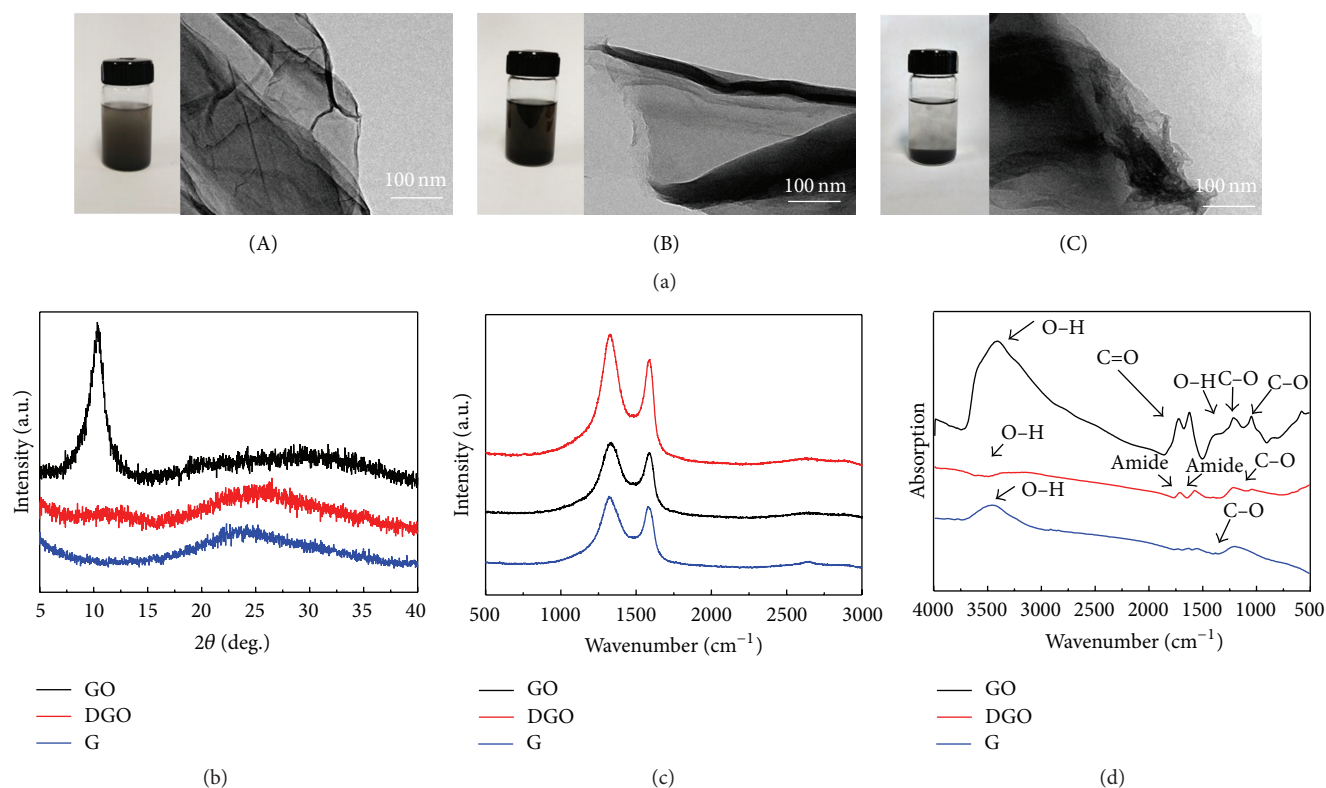


FIGURE 2: Characterization of GO, DGO, and G. (a) Digital photographs of aqueous dispersions (left) and TEM images (right) of (A) GO, (B) DGO, and (C) G. (b) XRD patterns. (c) Raman spectra. (d) FTIR spectra of GO, DGO, and G.

100 nm was achieved on 1 wt.% DGO/BG; relatively speaking, 5 wt.% DGO/BG composite resulted in more heterogeneous microscale topography with nucleation of BG particles on GO (Figures 3(b)(C) and 3(c)(C)). It should be notified that BG particles appeared to be melted and more aggregated and at 1200°C, besides fusion and densification, there is also an increase in the particles' size (Figure 3(a)(D)).

Raman spectrum (Figure 4(c)) showed that the characteristic peak of BG is at $\sim 850\text{ cm}^{-1}$. DGO has two broad peaks known as G and D bands ($\sim 1590\text{ cm}^{-1}$ and $\sim 1335\text{ cm}^{-1}$, resp.). Both 1 wt.% DGO/BG and 5 wt.% DGO/BG have three broad peaks including the characteristic peaks of DGO and BG without apparent shift, suggesting that these characteristic bands were not destroyed during the functionalization process. EDS spectra (Figure 4(b)) showed that C and O elements were detected in pure DGO, the elements of C, O, Si, and Ca were detected in pure BG, and all of these elements can be detected in 1 wt.% DGO/BG and 5 wt.% DGO/BG with different ratio. These results indicated that functionalization of GO with BG has yielded DGO/BG composite scaffold.

3.3. Evaluation and Biological Properties of DGO/BG

3.3.1. Adhesion and Spreading Patterns of rBMSCs on Bioactive DGO/BG. rBMSCs cell morphology on different substrates after 3 h and 1 day of culture was observed and counted by CLSM after immunofluorescent staining (Figure 5). At 3 h, the rBMSCs presented a round shape on all substrates

(Figure 5(a)). The cell area was slightly wider on the 1 wt.% DGO/BG scaffold than other groups. After 1 day, cells cultivated on 1 wt.% and 5 wt.% DGO/BG scaffold showed more spreading, larger area, and more confluence. Cells on DGO and BG substrates showed spindle-shaped morphology with constricted cell area (Figures 5(a) and 5(c)).

3.3.2. rBMSCs Viability on DGO/BG. Figure 5(e) showed the cell viability of rBMSCs cultured on various samples at 3 h and 1 day. Cell initial adhesion on 1 wt.% DGO/BG yielded the best results followed by 5 wt.% DGO/BG. There was no significant difference between pure BG and 5 wt.% DGO/BG; both of them facilitate the cell initial adhesion, while the cell initial adhesion showed decrease on pure DGO.

3.3.3. Osteogenic Differentiation of rBMSCs on DGO/BG. BMP2, BSP, RUNX2, and OPN mRNA expression profiles at 7 days are shown in Figure 6. DGO/BG composites promoted higher expression of selected osteogenic genes. When compared to pure DGO and BG, 1 wt.% DGO/BG yielded the best results. BMP2, OPN, and RUNX2 were chosen to have immunofluorescence staining (Figure 7). All of samples allowed for osteogenic differentiation of rBMSCs but led to different differentiation characteristics. The quantitative results demonstrated that 1 wt.% DGO/BG induced significantly higher expression levels of OPN and RUNX2 compared to other samples. DGO and BG substrates show similar osteogenic differentiation propensity.

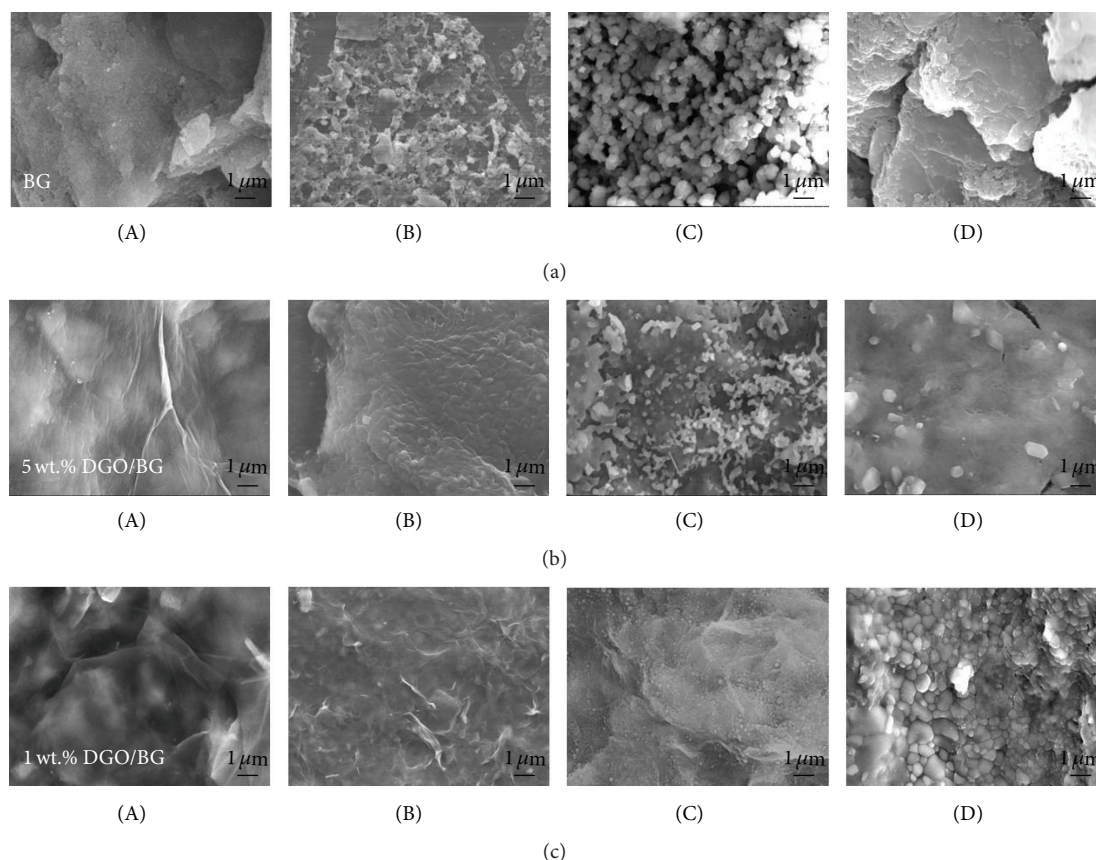


FIGURE 3: SEM images of DGO/BG composites with different loading ratio and reaction temperature. BG (a), 5 wt.% DGO/BG (b), and 1 wt.% DGO/BG (c) synthesized with different reaction temperatures: (A) 600°C, (B) 800°C, (C) 1000°C, and (D) 1200°C.

4. Discussion

Since the discovery of GO, much attention has been paid on improvement of its potential risks to biological systems so as to extend its application in biomedicine. The GO resulted hemolysis and cytotoxicity could be directly associated with its surfactant-like chemical structure with hydrophilic edges (ionized carboxyl groups) and hydrophobic plane (unoxidized sp^2 carbon skeleton), leading to strong electrostatic and hydrophobic interactions between GO and cell membrane. To enhance the biocompatibility of GO, dopamine (DA), a mussel-adhesive-protein inspired molecule, was used to partly reduce the ionized carboxyl groups on GO in this work.

TEM showed GO and DGO sheets have the typical fold morphology. While following the chemical reduction, G sheets displayed a more crumpled and wrinkled structure than GO and DGO, which is due to the lack of mutually exclusive polar groups; graphene atomic layers can stick together more easily by the van der Waals force.

The XRD showed a decrease of interlayer spacing from 0.78 nm to 0.39 nm, indicating that removal of oxygen and water from the interlayer occurred during reduction and modification. This broad peak also suggested a loss of the long range order in graphene. As indicated in Raman, the increase of the intensity ratio of the D band and G band

(ID/IG) was corresponding to high level defects with the insertion of functional groups during the modification of graphite oxide. Furthermore, the broad bands of GO and DGO ranging from 3400 to 3500 cm^{-1} shown in FTIR were corresponding to the O-H stretching vibration of adsorbed water molecules. The oxygen-containing functional groups of GO were revealed by the bands at 1054, 1226, 1617, and 1719 cm^{-1} . These bands can be assigned to the C-O stretching vibration, C-O-H deformation vibration, C=C stretching vibration, and C=O stretching vibration of COOH group, respectively [28, 29]. The bands associated with oxygen-containing functional groups decreased or disappeared significantly after reduction. Peak located at 1635 and 1558 cm^{-1} in the FTIR spectrum of DGO corresponds to the vibration of amide. Furthermore, the absorption peak of hydroxyl and epoxy group decreased after modification because of the reaction of phenolic hydroxyl group on amide and functional groups on GO and the part reduction of GO by amide. The FTIR results further agree with the XRD analyses results. Taken together, the XRD, Raman, and FTIR spectrums indicated that successful removal of oxygen and water from the interlayer occurred during reduction and high level defects with the insertion of functional groups during the modification of graphite oxide. As an amphiphilic molecule, DA has been modified onto various biopolymers,

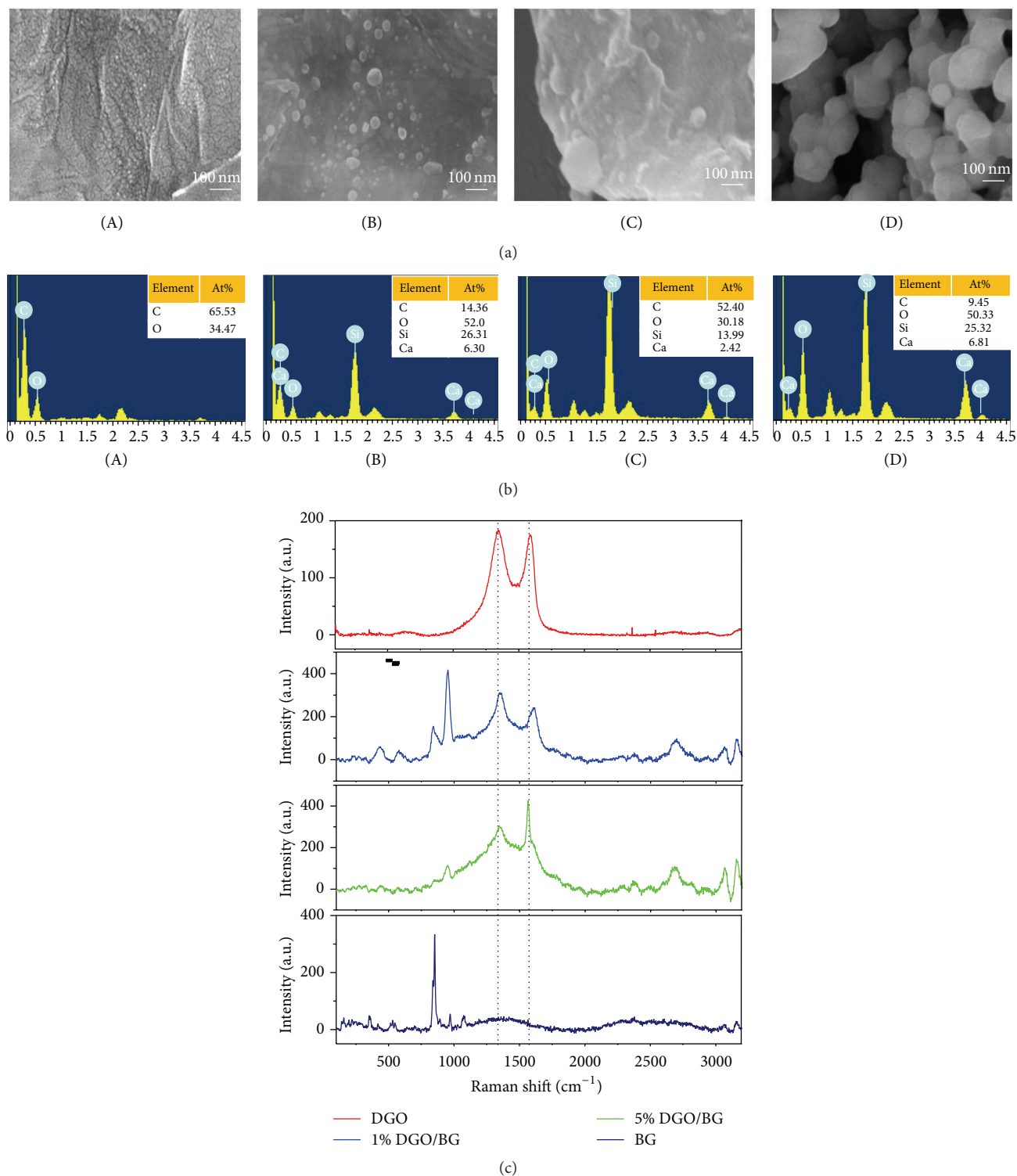


FIGURE 4: SEM images (a), EDS spectra (b), and Raman spectra (c) of different samples with 1000°C reaction temperature: (A) DGO, (B) 1 wt.% DGO/BG, (C) 5 wt.% DGO/BG, and (D) BG.

and the as-prepared biopolymers exhibited excellent adhesive ability to many kinds of solid surfaces. More recently, DA has been found to connect with GO by π -stacking. In our experiment, DA modification was found to enhance the

dispersion stability of GO, and it might also provide catechol groups to facilitate subsequent nucleation of BG on GO.

To improve the bioactivity of DGO in osteogenesis, BG was used in further surface functionalization due to its

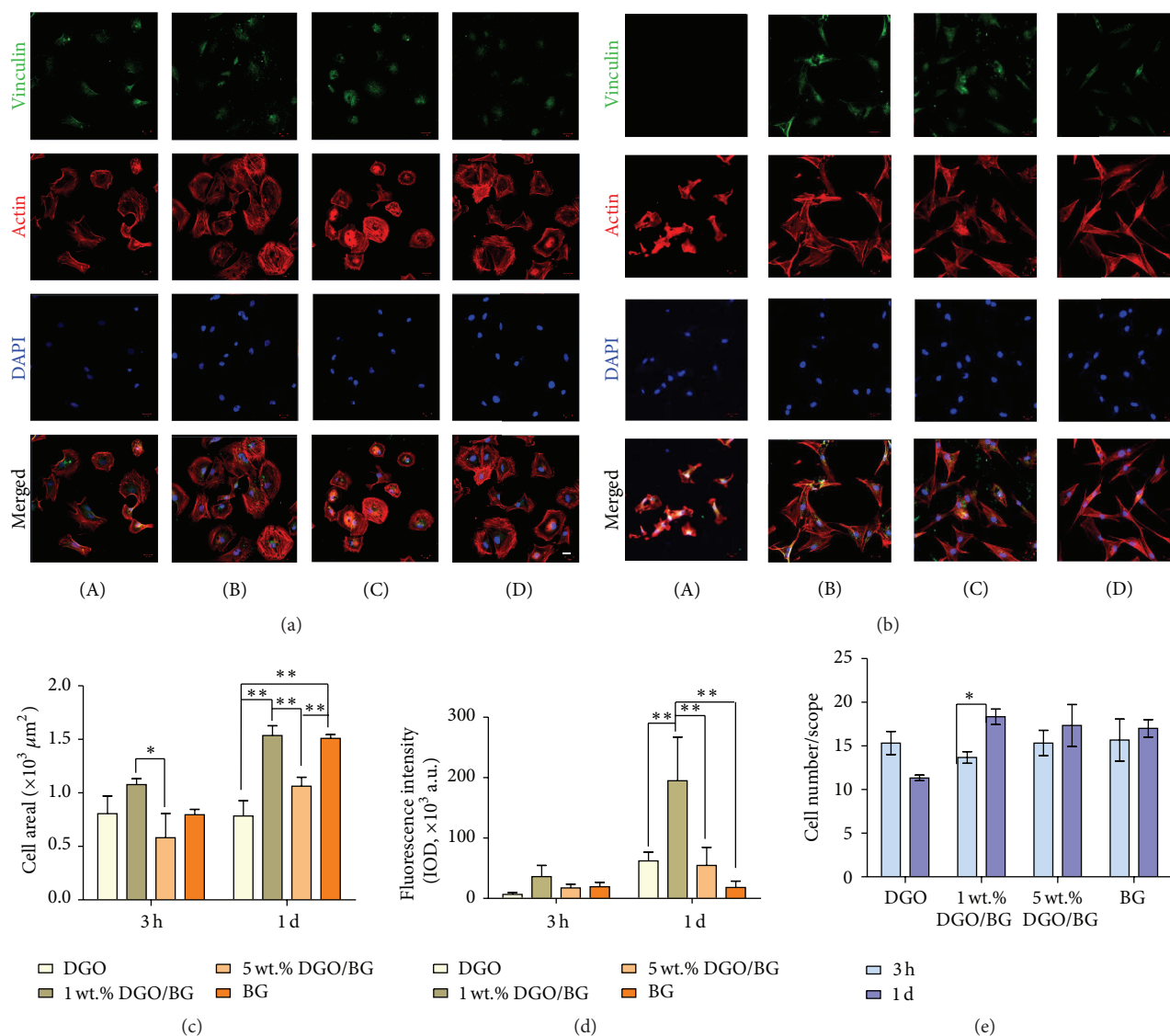


FIGURE 5: Adhesion and spreading patterns of rBMSCs on various samples. Immunostaining of vinculin (green), actin (red), and nuclei (blue) for rBMSCs cultured on the samples for 3 hours (a) and 1 day (b): (A) DGO, (B) 1 wt.% DGO/BG, (C) 5 wt.% DGO/BG, and (D) BG. Scale bars, 20 μm. The quantitative analysis of cell spreading area (c) and vinculin (d) on different samples. (e) Initial adhesion was evaluated by counting the number of live cells per unit area on each substrate at 3 hours and 1 day, and each group was repeated for three times (* $p < 0.05$, ** $p < 0.01$).

excellent osteoinductivity and osteoconductivity [21, 30, 31]. Previously, biopolymers such as polysaccharide, protein, and DNA have been used to promote the bioactivity of GO. However, in these studies, the biopolymer loading ratio, the elution of the adsorbed biopolymer, and the 2D surface morphology were difficult to be controlled. In our studies, the influences of different DGO/BG loading ratio and the sol-gel-melting technique on physical and chemical features of final composites were exquisitely controlled. As indicated in Figure 3, BG particles only emerged above reaction temperature of 600°C with sol-gel method, which proved the previous studies demonstrating that the nucleation of BG was impeded by low temperature [32]. Heterogeneous microscale particles presented on 5 wt.% DGO/BG composite scaffold,

while homogeneous distribution of nanospheric particles with diameter ranging from 50 to 100 nm was achieved at 1000°C on 1 wt.% DGO/BG. EDS spectra indicated that these particles are BG. These results indicated that the addition of DGO had generated the porous inner microstructure and coarse surface morphology for BG, which was attributed to the microphase separation between DGO and BG in the blend solution. During the carbonization and pore structure formation, BG precursors transformed into BG nanoparticles by thermodynamic driving force [33]. EDS spectra also showed that DGO/BG scaffold possessed the C element of GO and Si and Ca elements of BG. Raman spectrum demonstrated that DGO/BG composite scaffold has the characteristic peaks of both DGO and BG without

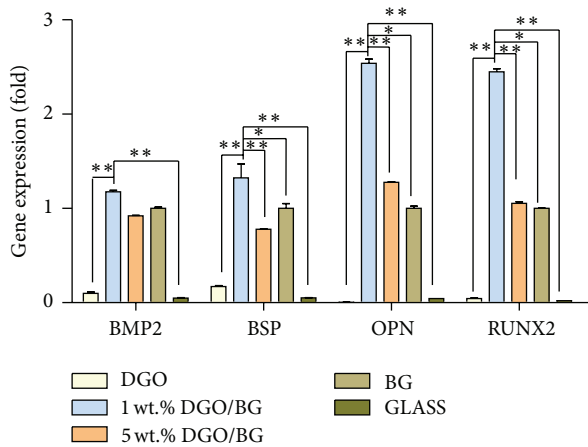


FIGURE 6: Gene expression levels of BMP2, BSP, OPN, and RUNX2 in rBMSCs cultured for 7 days (* $p < 0.05$, ** $p < 0.01$).

apparent shift, suggesting that these characteristic bands were not destroyed during the functionalization process. These results indicated that with unique topographical DGO/BG composite scaffolds were achieved with controlled DGO/BG loading ratio and sol-gel-melting technique.

As the first fundamental step of interaction with scaffold, cell adhesion could significantly impact the spreading morphology and capacity of cell proliferation and differentiation [34, 35]. Therefore, the cell adhesion and subsequent growth are essentially important markers to determine whether materials could be used as scaffolds in bone regeneration. In this study, to investigate whether the functionalization of BG on DGO would influence the initial behavior of rBMSCs, we examined the cell adhesion and spreading patterns by immunofluorescent staining at 3 h and 1 day. The immunofluorescent staining showed that rBMSCs cultivated on DGO/BG scaffolds are more favorable to rBMSCs than DGO and BG substrates with respect to cell adhesion. The stable adhesion of stem cells on substrates is a fundamental and important requirement for regulating stem cell functions. Furthermore, the qualified morphological analysis suggests that 1 wt.% and 5 wt.% DGO/BG scaffolds present much higher cell spreading area. It is widely accepted that enhanced cell spreading is an important factor to be considered for enhancing differentiation of stem cells. Additionally, cells on the DGO/BG substrates have higher cell viability than those on pure DGO and BG substrates regardless of the incorporated DGO/BG molar ratio. These results suggested that the incorporation of DGO and BG has improved the biocompatibility of both of them, yielding a suitable environment for the rBMSCs growth.

A growing number of studies suggested that the physical geometry as well as chemical composition of substrates could direct specific tissue lineages of stem cells [36]. Since as achieved DGO/BG has unique properties including topographic features and bioactive chemical components, we expected that DGO/BG scaffold would influence the differentiation of stem cells. Our study shows that all the DGO, BG, and DGO/BG scaffolds can be used to

modulate the osteogenesis of rBMSCs. In particular, 1 wt.% DGO/BG scaffold exhibits significantly highest osteogenic differentiation propensity compared to those on the other substrates, indicating that the 1 wt.% DGO/BG scaffold may have great potential for bone defect healing applications. According to the previous research, the effect of GO substrate on promoting stem cell differentiation was intimately related to its high Young's modulus [37] and the surface oxygen functional groups as well as proteins absorption [10, 38, 39]. On one hand, the favorable osteogenic lineage effect of BG was clarified to be ascribed to the release and exchange of critical concentrations of soluble Si and Ca ions. The BG nanoparticles with large surface area/volume ratio have been reported to facilitate quick ions release and high mineralization and have a significant function in genetic control over the cellular response to favor osteogenesis. Meanwhile, extensive works have demonstrated that the BG concentration is critical in cellular response to BG containing composites [40]. Moreover, the growth and differentiation of osteoblast-like cells and the kinetics of Ca-P chemistry on PLGA/BG and PDLA/BG films were shown to depend on BG content. As such, although a combination of factors including stiffness, reactive functional groups, and absorption of biomolecules on DGO/BG composite scaffolds could affect the rBMSCs osteogenic behaviors, the unique nanotopography and high bioactive BG content of 1 wt.% DGO/BG scaffold might provide more chances compared to microtopographical 5 wt.% DGO/BG to promote stem cell osteogenic differentiation. These findings suggest that the DGO/BG composite scaffolds could be used as an enabling tool for modulating the osteogenesis of stem cells.

5. Conclusions

In this study, from evaluation of the biocompatibility of DGO/BG, we found that DGO/BG hybrid scaffolds containing different content of DGO could enhance rBMSCs' adhesion, spreading, and differentiation. The TEM, XRD, Raman, and FTIR spectrums indicated successful synthesis of the typical fold morphology DGO by insertion of functional groups during the modification of graphite oxide. The dopamine modification enhanced the dispersion stability of GO and might provide catechol groups to facilitate subsequent nucleation of BG on DGO with sol-gel method. Scanning electron microscopy (SEM) showed that unique homogeneous nanospheric topography could be achieved on GO by controlling the DGO/BG molar ratio and reaction temperature. The Raman and EDS characterization confirmed the modification of BG on DGO. Higher cellular activities of cell adhesion and spreading were achieved on DGO/BG scaffolds compared to pure DGO and BG substrates. Enhanced cell adhesion and spreading were achieved on 1 wt.% and 5 wt.% DGO/BG scaffolds, indicating the favorable biocompatibility of DGO/BG. The highest expression level of osteogenic markers including BMP2, OPN, and RUNX2 was observed. The significantly high osteogenic markers expression on DGO/BG scaffold suggests that the proposed DGO/BG scaffolds could promote the osteogenic differentiation of rBMSCs. Taken together, we envision that the DGO/BG

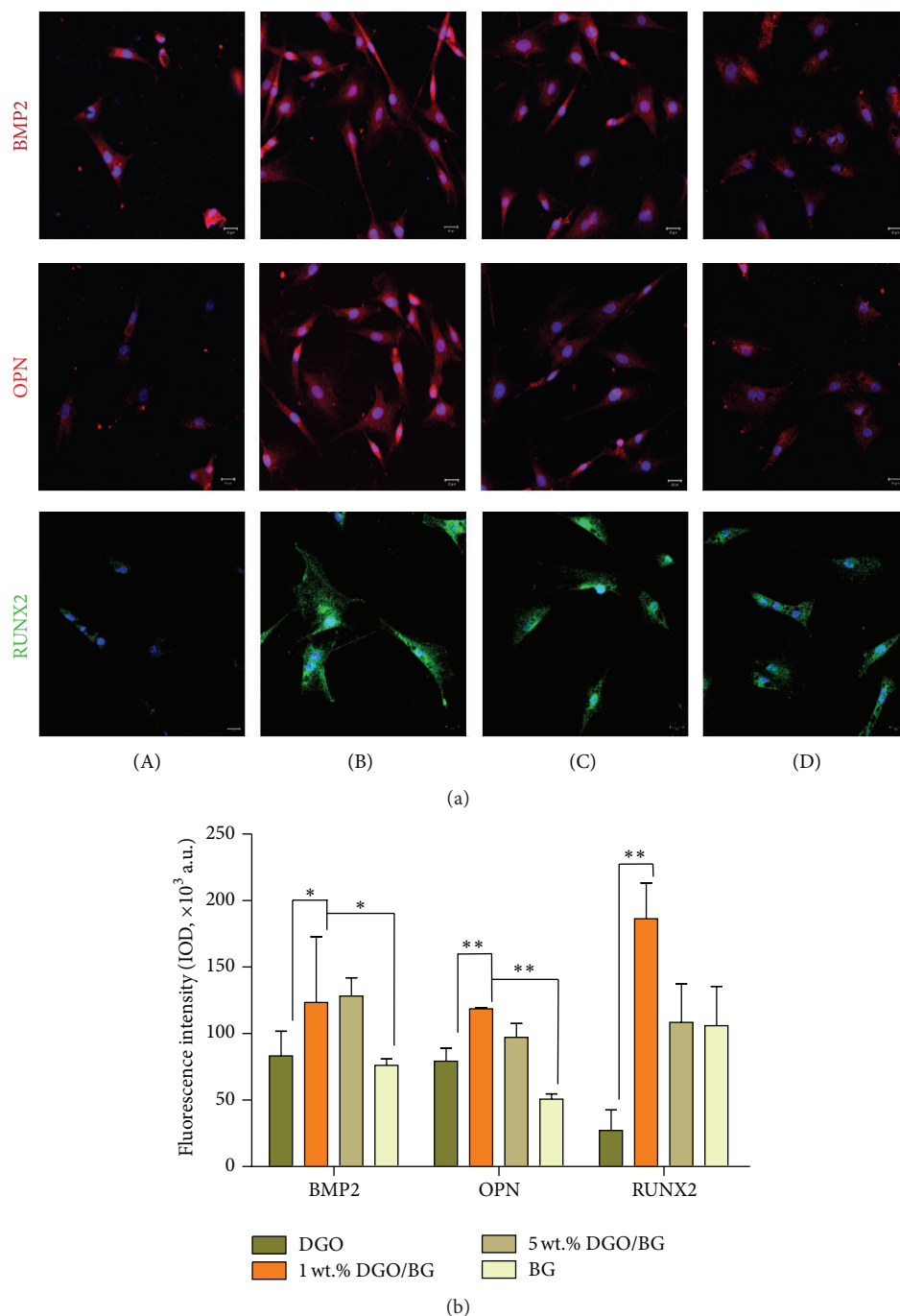


FIGURE 7: Semiquantitative analysis of GO/BG stimuli induced osteogenic differentiation of rBMSCs. (a) Immunostaining of osteogenic proteins BMP2, OPN, and RUNX2 on different samples at 7 days: (A) DGO, (B) 1 wt.% DGO/BG, (C) 5 wt.% DGO/BG, and (D) BG. Scale bars, 20 μm . (b) Quantification of mean immunofluorescence intensities of BMP2, OPN, and RUNX2 in groups as defined in (a). All measurements were performed in triplicate and analyzed by one-way ANOVA with Tukey's posttest to account for multiple comparisons. Data were plotted as mean; error bars are SEM. BMP2, red; OPN, red; RUNX2, green (* $p < 0.05$, ** $p < 0.01$).

scaffold will open avenues for next-generation graphene applications in the realm of functional biomaterial. However, further studies *in situ* are still needed to evaluate their efficacy in promoting bone regeneration and neovascularization.

Competing Interests

The authors declare that there are no competing interests regarding the publication of this paper.

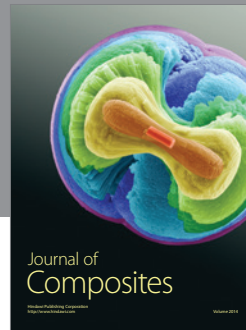
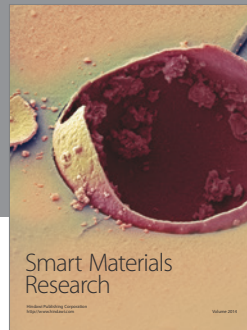
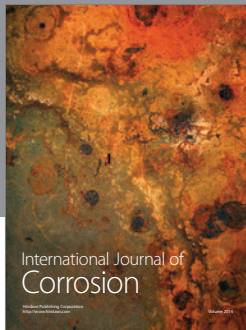
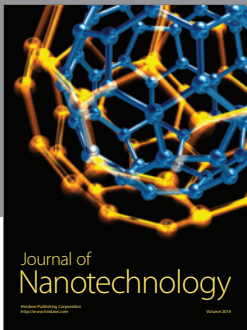
Acknowledgments

This work was financially supported by the National Natural Science Foundation of China (81425007 and 51502005), the National Basic Science Research Program (2012CB933900), and the National High Technology Research and Development Program of China (2015AA033601). Additionally, the authors also acknowledge the support of the Peking University-Tsinghua University Joint Center and Beijing University of Chemical Technology for Life Sciences.

References

- [1] Q. Li, L. Liu, S. Zhang et al., "Modulating $A\beta_{33-42}$ peptide assembly by graphene oxide," *Chemistry—A European Journal*, vol. 20, no. 24, pp. 7236–7240, 2014.
- [2] J. Wang, Y. Cao, Q. Li, L. Liu, and M. Dong, "Size effect of graphene oxide on modulating amyloid peptide assembly," *Chemistry—A European Journal*, vol. 21, no. 27, pp. 9632–9637, 2015.
- [3] Z. M. Markovic, L. M. Harhaji-Trajkovic, B. M. Todorovic-Markovic et al., "In vitro comparison of the photothermal anticancer activity of graphene nanoparticles and carbon nanotubes," *Biomaterials*, vol. 32, no. 4, pp. 1121–1129, 2011.
- [4] D. Depan, J. Shah, and R. D. K. Misra, "Controlled release of drug from folate-decorated and graphene mediated drug delivery system: synthesis, loading efficiency, and drug release response," *Materials Science and Engineering C*, vol. 31, no. 7, pp. 1305–1312, 2011.
- [5] Z. Liu, J. T. Robinson, S. M. Tabakman, K. Yang, and H. Dai, "Carbon materials for drug delivery & cancer therapy," *Materials Today*, vol. 14, no. 7-8, pp. 316–323, 2011.
- [6] Z. Wang, Y. Gao, J. Xia, F. Zhang, Y. Xia, and Y. Li, "Synthesis and characterization of glycyrrhizin-decorated graphene oxide for hepatocyte-targeted delivery," *Comptes Rendus Chimie*, vol. 15, no. 8, pp. 708–713, 2012.
- [7] K. S. Novoselov, A. K. Geim, S. V. Morozov et al., "Electric field effect in atomically thin carbon films," *Science*, vol. 306, no. 5696, pp. 666–669, 2004.
- [8] L. L. Hench and J. M. Polak, "Third-generation biomedical materials," *Science*, vol. 295, no. 5557, pp. 1014–1017, 2002.
- [9] W. Wei and X. Qu, "Extraordinary physical properties of functionalized graphene," *Small*, vol. 8, no. 14, pp. 2138–2151, 2012.
- [10] W. C. Lee, C. H. Y. X. Lim, H. Shi et al., "Origin of enhanced stem cell growth and differentiation on graphene and graphene oxide," *ACS Nano*, vol. 5, no. 9, pp. 7334–7341, 2011.
- [11] J. Kim, K. S. Choi, Y. Kim et al., "Bioactive effects of graphene oxide cell culture substratum on structure and function of human adipose-derived stem cells," *Journal of Biomedical Materials Research Part A*, vol. 101, no. 12, pp. 3520–3530, 2013.
- [12] S. Some, S.-M. Ho, P. Dua et al., "Dual functions of highly potent graphene derivative-poly-L-lysine composites to inhibit bacteria and support human cells," *ACS Nano*, vol. 6, no. 8, pp. 7151–7161, 2012.
- [13] H. Liu, J. Cheng, F. Chen et al., "Gelatin functionalized graphene oxide for mineralization of hydroxyapatite: biomimetic and in vitro evaluation," *Nanoscale*, vol. 6, no. 10, pp. 5315–5322, 2014.
- [14] Y. Shi, M. Li, Q. Liu et al., "Electrophoretic deposition of graphene oxide reinforced chitosan-hydroxyapatite composite coatings for biomedical applications," *European Cells and Materials*, vol. 27, no. 3, article 48, 2013.
- [15] J. R. Jones, S. Lin, S. Yue et al., "Bioactive glass scaffolds for bone regeneration and their hierarchical characterisation," *Proceedings of the Institution of Mechanical Engineers Part H: Journal of Engineering in Medicine*, vol. 224, no. 12, pp. 1373–1387, 2010.
- [16] L. L. Hench, "Bioceramics—from concept to clinic," *Journal of the American Ceramic Society*, vol. 74, pp. 1487–1510, 1991.
- [17] T. Kokubo, H.-M. Kim, and M. Kawashita, "Novel bioactive materials with different mechanical properties," *Biomaterials*, vol. 24, no. 13, pp. 2161–2175, 2003.
- [18] L. L. Hench, "Bioceramics," *Journal of the American Ceramic Society*, vol. 81, no. 7, pp. 1705–1728, 1998.
- [19] J. R. Jones, "New trends in bioactive scaffolds: the importance of nanostructure," *Journal of the European Ceramic Society*, vol. 29, no. 7, pp. 1275–1281, 2009.
- [20] M. Tommila, A. Jokilampi, P. Terho, T. Wilson, R. Penttinen, and E. Ekholm, "Hydroxyapatite coating of cellulose sponges attracts bone-marrow-derived stem cells in rat subcutaneous tissue," *Journal of the Royal Society Interface*, vol. 6, no. 39, pp. 873–880, 2009.
- [21] S. Wang, X. Gao, W. Gong, Z. Zhang, X. Chen, and Y. Dong, "Odontogenic differentiation and dentin formation of dental pulp cells under nanobioactive glass induction," *Acta Biomaterialia*, vol. 10, no. 6, pp. 2792–2803, 2014.
- [22] C. Zhang, D. Cheng, T. Tang, X. Jia, Q. Cai, and X. Yang, "Nanoporous structured carbon nanofiber–bioactive glass composites for skeletal tissue regeneration," *Journal of Materials Chemistry B*, vol. 3, no. 26, pp. 5300–5309, 2015.
- [23] A. C. M. Renno, F. C. J. Van De Watering, M. R. Nejadnik et al., "Incorporation of bioactive glass in calcium phosphate cement: an evaluation," *Acta Biomaterialia*, vol. 9, no. 3, pp. 5728–5739, 2013.
- [24] W. S. Hummers and R. E. Offeman, "Preparation of Graphitic Oxide," *Journal of the American Chemical Society*, vol. 80, no. 6, p. 1339, 1958.
- [25] L. Zhao, L. Liu, Z. Wu, Y. Zhang, and P. K. Chu, "Effects of micropitted/nanotubular titania topographies on bone mesenchymal stem cell osteogenic differentiation," *Biomaterials*, vol. 33, no. 9, pp. 2629–2641, 2012.
- [26] C. H. Seo, H. Jeong, K. S. Furukawa, Y. Suzuki, and T. Ushida, "The switching of focal adhesion maturation sites and actin filament activation for MSCs by topography of well-defined micropatterned surfaces," *Biomaterials*, vol. 34, no. 7, pp. 1764–1771, 2013.
- [27] C. Wu, L. Xia, P. Han et al., "Graphene-oxide-modified β -tricalcium phosphate bioceramics stimulate in vitro and in vivo osteogenesis," *Carbon*, vol. 93, pp. 116–129, 2015.
- [28] Q. Q. Zhuo, J. Gao, M. Peng et al., "Large-scale synthesis of graphene by the reduction of graphene oxide at room temperature using metal nanoparticles as catalyst," *Carbon*, vol. 52, pp. 559–564, 2013.
- [29] J. Dong, J. Weng, and L. Z. Dai, "The effect of graphene on the lower critical solution temperature of poly(*N*-isopropylacrylamide)," *Carbon*, vol. 52, pp. 326–336, 2013.
- [30] J. R. Jones, P. Sepulveda, and L. L. Hench, "Dose-dependent behavior of bioactive glass dissolution," *Journal of Biomedical Materials Research*, vol. 58, no. 6, pp. 720–726, 2001.
- [31] J. Wilson, G. H. Pigott, F. J. Schoen, and L. L. Hench, "Toxicology and biocompatibility of bioglasses," *Journal of Biomedical Materials Research*, vol. 15, no. 6, pp. 805–817, 1981.

- [32] Y. Yin, F. Ye, J. Cui, F. Zhang, X. Li, and K. Yao, "Preparation and characterization of macroporous chitosan-gelatin/ β -tricalcium phosphate composite scaffolds for bone tissue engineering," *Journal of Biomedical Materials Research—Part A*, vol. 67, no. 3, pp. 844–855, 2003.
- [33] C. Kim, Y. I. Jeong, B. T. N. Ngoc et al., "Synthesis and characterization of porous carbon nanofibers with hollow cores through the thermal treatment of electrospun copolymeric nanofiber webs," *Small*, vol. 3, no. 1, pp. 91–95, 2007.
- [34] M. L. Rodriguez, P. J. McGarry, and N. J. Sniadecki, "Review on cell mechanics: experimental and modeling approaches," *Applied Mechanics Reviews*, vol. 65, no. 6, Article ID 060801, 2013.
- [35] S. R. Frenkel, R. M. Clancy, J. L. Ricci, P. E. Di Cesare, J. J. Rediske, and S. B. Abramson, "Effects of nitric oxide on chondrocyte migration, adhesion, and cytoskeletal assembly," *Arthritis and Rheumatism*, vol. 39, no. 11, pp. 1905–1912, 1996.
- [36] H. Nikukar, S. Reid, P. M. Tsimbouri, M. O. Riehle, A. S. G. Curtis, and M. J. Dalby, "Osteogenesis of mesenchymal stem cells by nanoscale mechanotransduction," *ACS Nano*, vol. 7, no. 3, pp. 2758–2767, 2013.
- [37] C. Yang, M. W. Tibbitt, L. Basta, and K. S. Anseth, "Mechanical memory and dosing influence stem cell fate," *Nature Materials*, vol. 13, no. 6, pp. 645–652, 2014.
- [38] W.-J. Li, R. Tuli, X. Huang, P. Laquerriere, and R. S. Tuan, "Multilineage differentiation of human mesenchymal stem cells in a three-dimensional nanofibrous scaffold," *Biomaterials*, vol. 26, no. 25, pp. 5158–5166, 2005.
- [39] M. Li, Q. Liu, Z. Jia et al., "Graphene oxide/hydroxyapatite composite coatings fabricated by electrophoretic nanotechnology for biological applications," *Carbon*, vol. 67, pp. 185–197, 2014.
- [40] P. Valerio, M. M. Pereira, A. M. Goes, and M. F. Leite, "The effect of ionic products from bioactive glass dissolution on osteoblast proliferation and collagen production," *Biomaterials*, vol. 25, no. 15, pp. 2941–2948, 2004.



Hindawi

Submit your manuscripts at
<http://www.hindawi.com>

